Supplementary Information

Improving the Charge Transport in Self-assembled Monolayer Field-effect Transistors – From Theory to Devices

Christof M. Jäger, Thomas Schmaltz, Michael Novak, Artoem Khassanov, Alexei Vorobiev, Matthias Hennemann, Andreas Krause, Hanno Dietrich, Dirk Zahn, Andreas Hirsch, Marcus Halik and Timothy Clark

Contents

Supplementary Table S1: Setup and results from MD simulations.

	MD100%	**MD25%**	**MD33%**	**MD38%**	**MD50%**
% of 1	100	25	33	38	50
surface coverage (nm^{-2})	0.9	3.6	2.7	2.3	1.8
molecules per periodic cell (1:2)	25:0	25:75	25:50	25:40	25:25
accessible layer thickness (nm)[a]	1.22±0.44	2.00±0.50	1.75±0.48	1.56±0.51	1.45±0.39
mean fullerene distance to substrate (nm)	0.95±0.31	1.74±0.25	1.44±0.30	1.35±0.33	1.14±0.28
mean inclination angle of alkane chain of 1(°)	18.15	55.7	53.9	37.6	35.1
mean inclination angle of alkane chain of 2(°)	-	57.2	46.6	38.6	27.6

[a] The mean accessible layer thickness is calculated from the averaged surface accessible by a sphere with a radius of 0.2 nm. The averaged surface was calculated from 80 ns simulation (after 20 ns equilibration), taking snapshots every 50 ps.

To obtain a densely packed monolayer of aliphatic PAs, molecules of **2** were placed in a rhombic arrangement above the surface. Starting from this configuration, the molecules in the center of two of the unit cells in a 2×2 superstructure of the previous lattice were replaced by **1**. This leads to a mixed SAM with a content of 25% **1** (MD25%) and an occupation of 69.4% of the aluminum atoms at the surface.

During a short relaxation (20,000 steps steepest descent), the PA-anchor groups were allowed to find suitable binding sites. Because of incomplete occupation of possible binding sites and the mismatch of the rhombic lattice and the lattice of the underlying aluminum oxide, the relaxation yielded a more disordered topology with trenches and vacancies. Subsequently, the system was heated to 300 K in steps of 20 K with a simulation time of 12.5 ps per temperature step followed by 100 ns MD

simulation. The last 80 ns of the simulations were used for structural and dynamic analyses and snapshots from this period for subsequent quantum mechanical calculations.

To yield denser monolayers of pure **1**, additional molecules were added after equilibration of MD50% in the case were surface anchor positions were directly accessible to additional PAs. Subsequently, all molecules of **2** were removed and the equilibration and production simulation was performed. Snapshots and analysis of this simulation are shown in Figure S2.

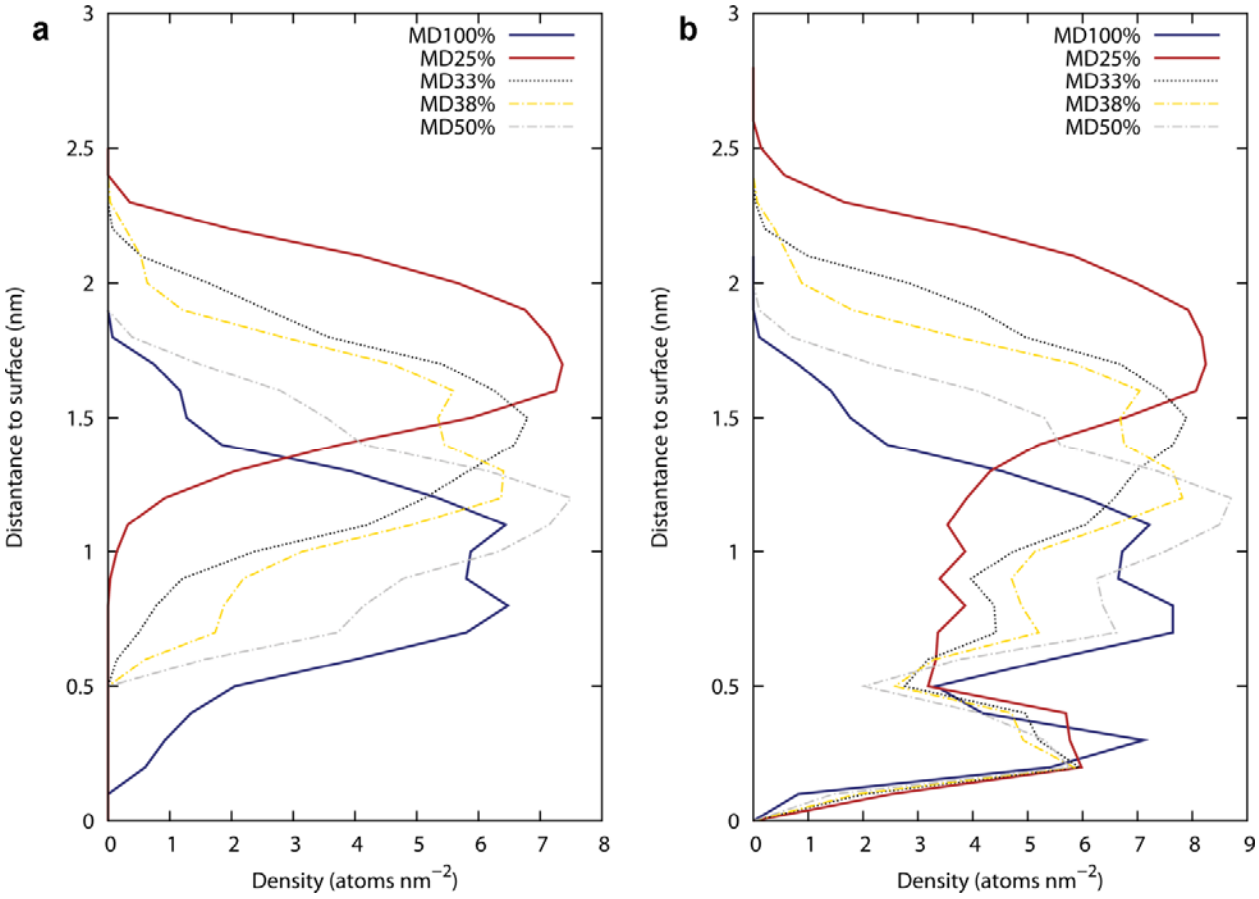

Supplementary Figure S1. Average atomic density derived from 80 ns (after 20 ns equilibration) simulation for **a** all fullerene atoms and **b** all atoms of differently mixed self-assembled monolayers.

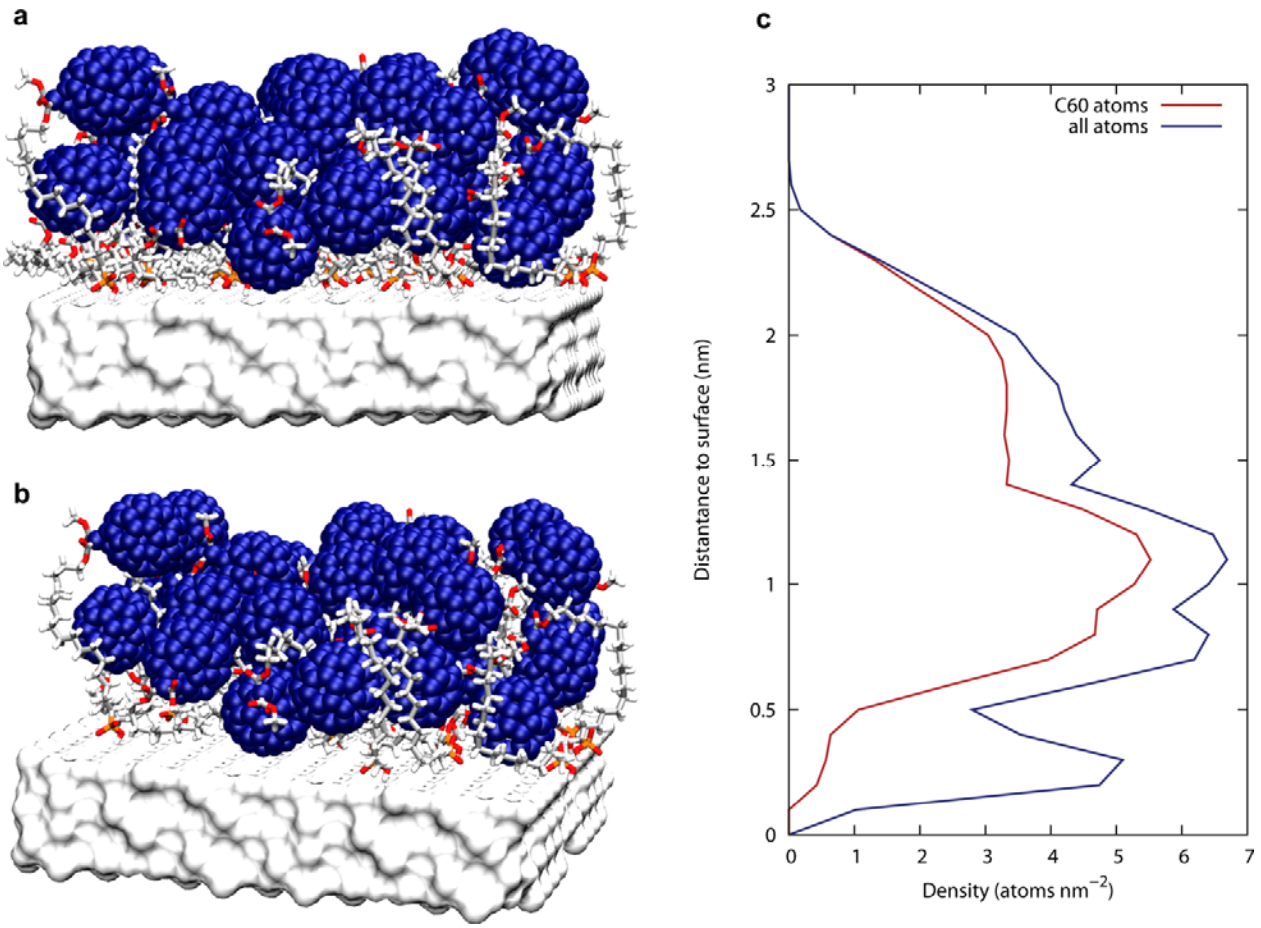

Supplementary Figure S2. A denser packing of a pure $C_{60}C_{18}$-PA in a MD simulation was achieved by substituting a 50:50 mixture after equilibration by removing and exchanging C_{10}-PA molecules to give a system of 32 $C_{60}C_{18}$-PA molecules. 5 ns equilibration reveal a significantly thicker and highly amorphous SAM compared to the less densely packed MD100%. The SAM has an average accessible layer thickness of 1.4±0.44 nm which is thinner than MD25% because of its amorphous character, but the absolute thickness is comparable (~2.5 nm). The mean fullerene atom distance to the surface is 1.3 nm with a broad distribution of fullerene atoms (rmsd: 0.43 nm) which agrees well with XRR measurements. The mean inclination angle of the alkyl chains is 30.3°. (a,b) Different views on a snapshot of the equilibrated SAM after 5 ns simulation. (c) Average atomic density from 5 ns simulation.

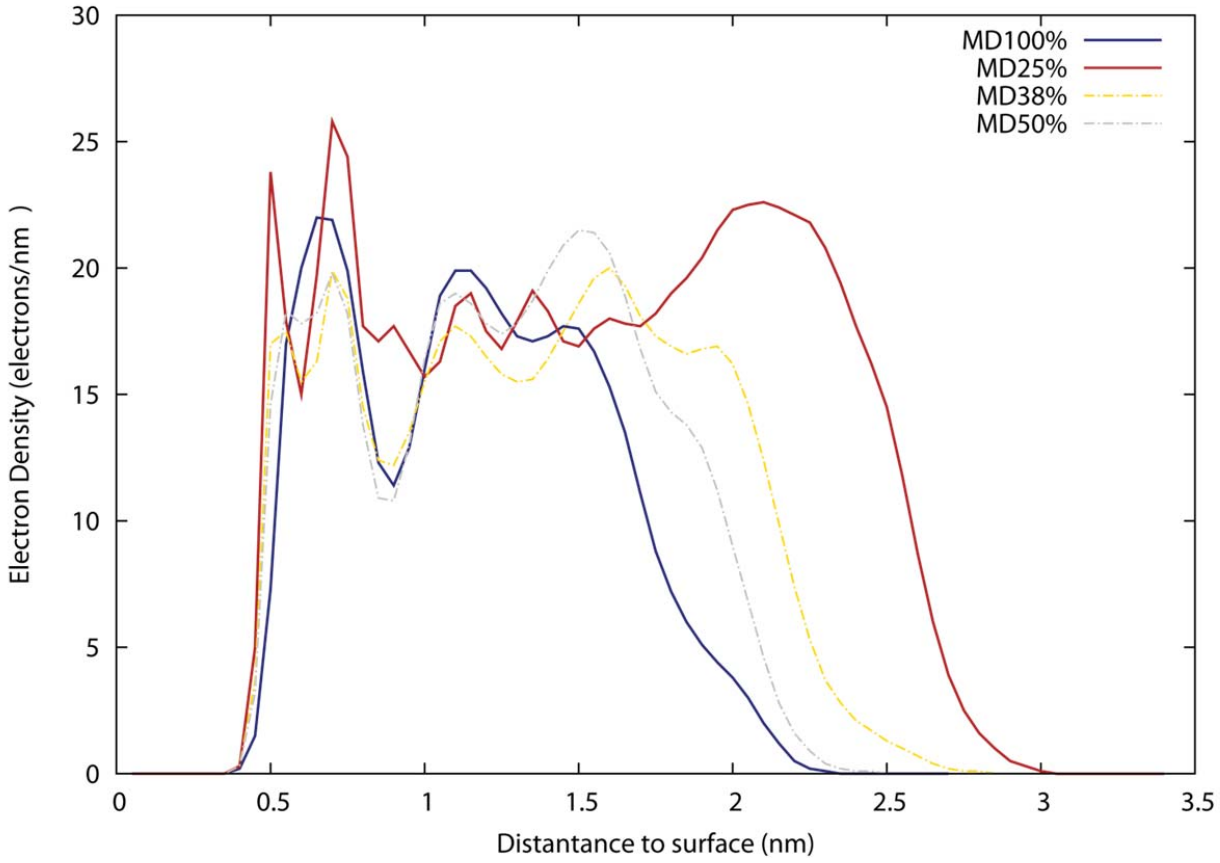

Supplementary Figure S3. Mean electron density profiles derived from 150 semiempirical AM1 single-point calculations per system.

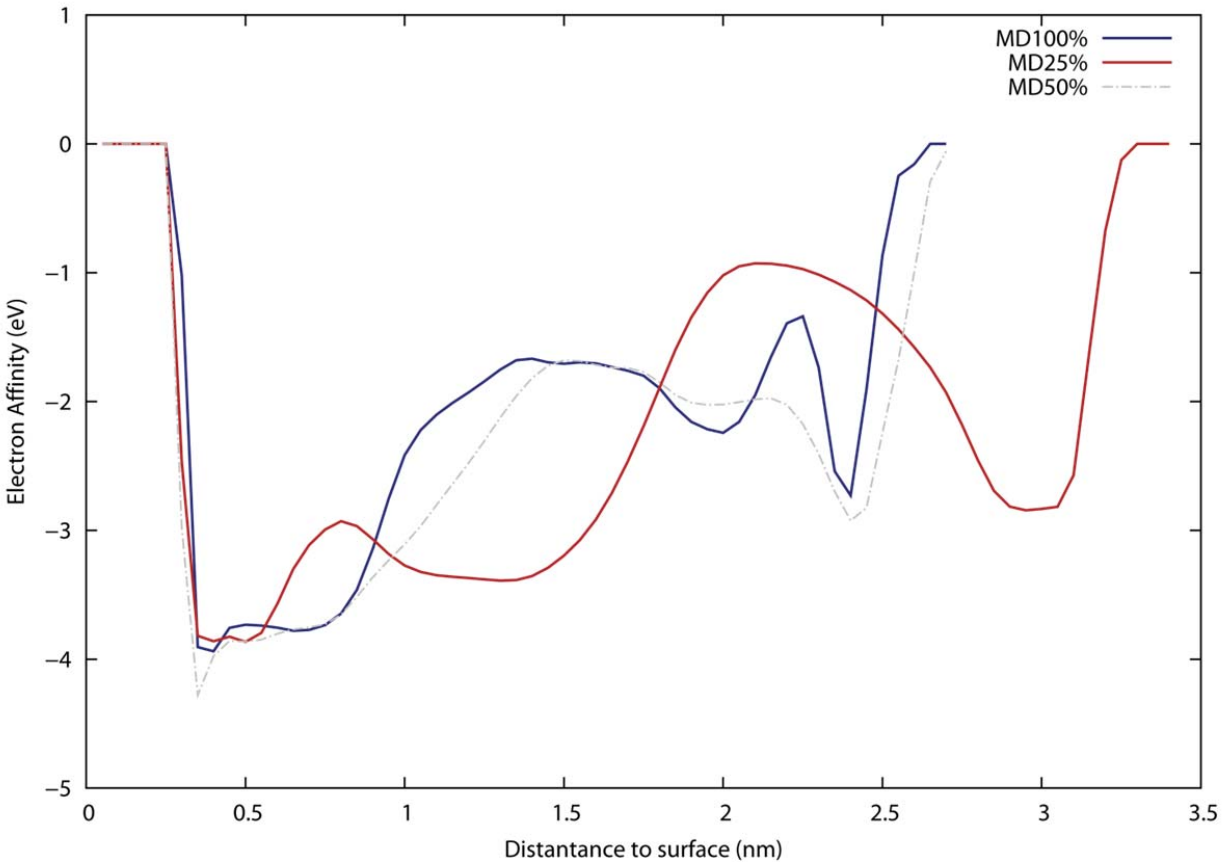

Supplementary Figure S4. Mean local electron affinity normal to the surface derived from 150 semiempirical AM1 single-point calculations per system.

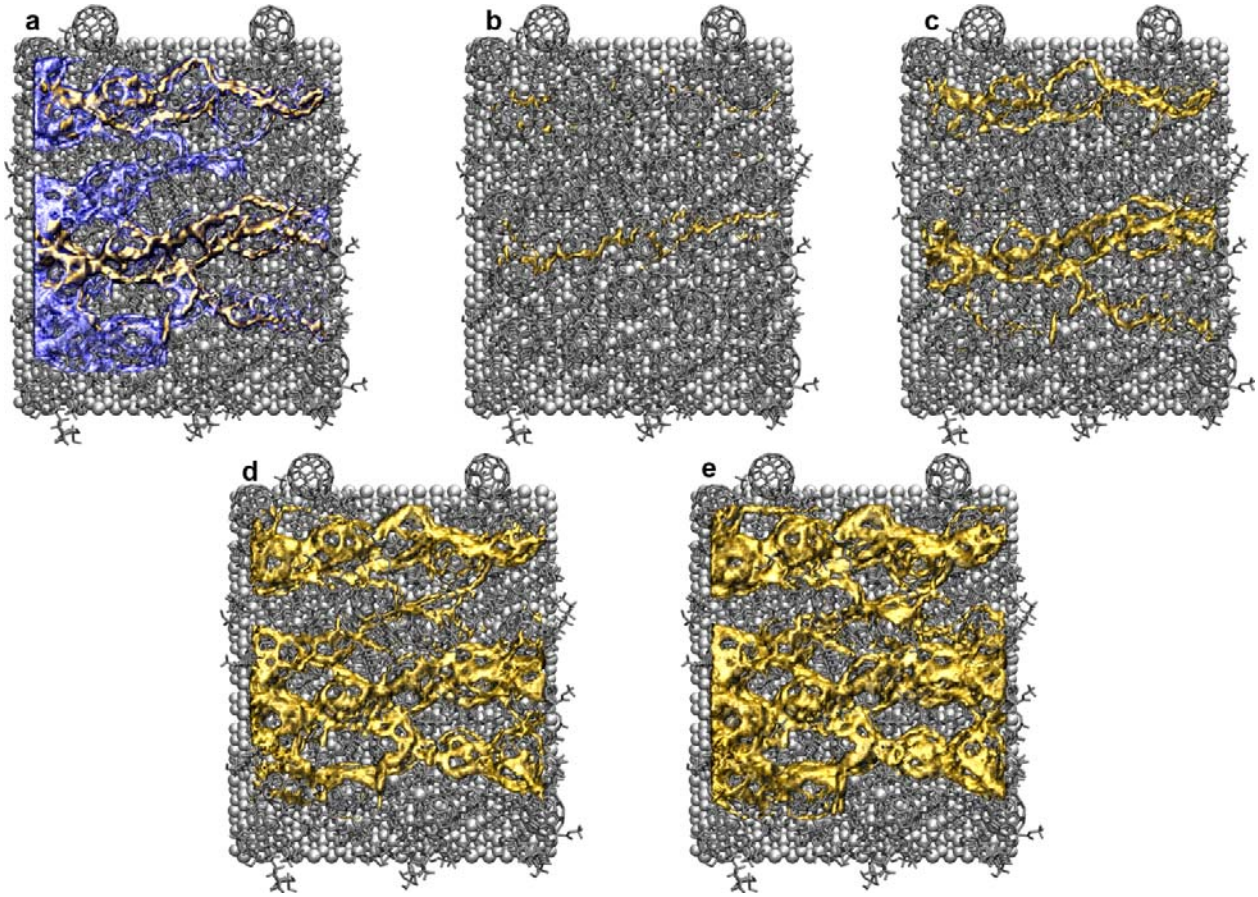

Supplementary Figure S5. To benchmark the Monte Carlo acceptance rate, the MC temperature was altered between 1000K and 3500K. (a) Crossing Monte Carlo electron-transfer paths shown in gold and trapped paths in blue for a snapshot of MD25%. SAM displayed in grey. (b-e) Crossing paths with different acceptance rates (b: 172 mV, c,a: 215 mV, d: 285 mV, e: 308 mV thermal voltage).

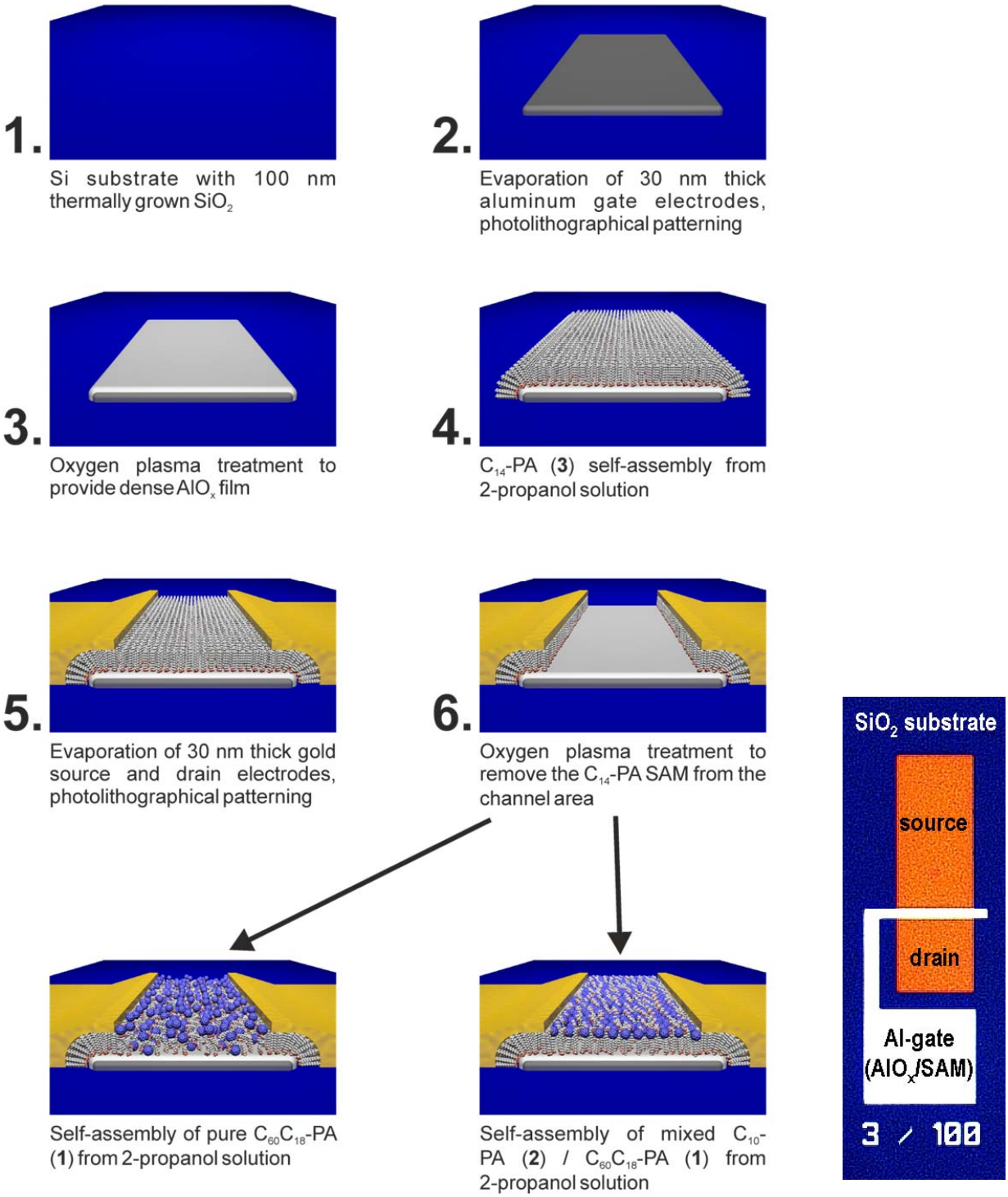

Supplementary Figure S6. Schematic diagram of the preparation process of pure $C_{60}C_{18}$-PA and mixed C_{10}-PA / $C_{60}C_{18}$-PA SAMFET devices and optical photograph of a fully processed device.

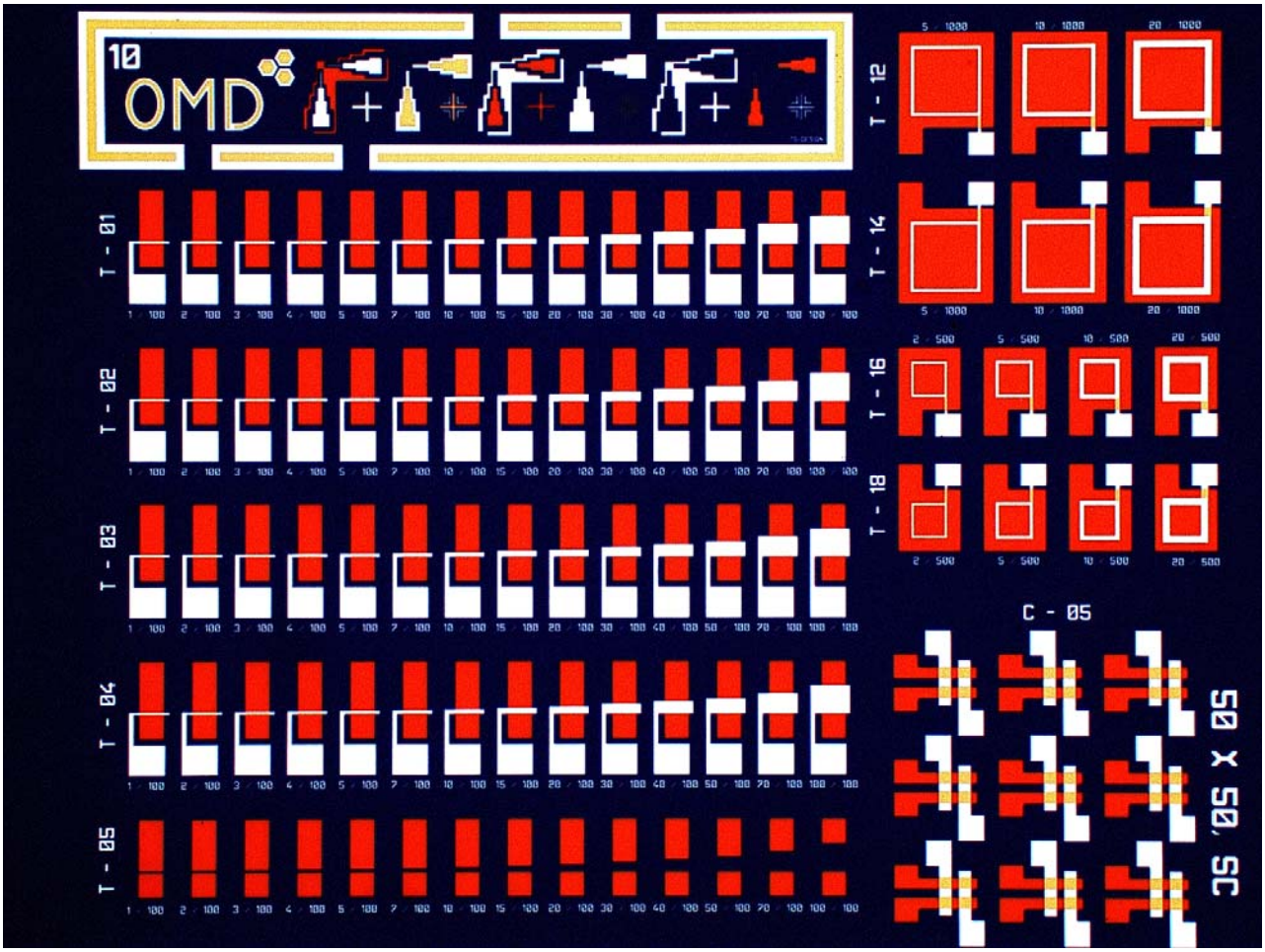

Supplementary Figure S7. Overview of a complete fully processed device taken with a CCD camera.

X-ray reflectivity experiments:

XRR experiments were performed at the ID10 Soft interfaces and coherent scattering beamline (EH1-LSIS) at the ESRF (Grenoble, France) with a photon wavelength of $\lambda = 1.55$ Å and a beam size of 50 µm x 500 µm after collimation with an incident flux on the sample in the order of 10^{11} photons/s. The specularly reflected X-rays and the parasitic background for correction were collected using a Vantec linear position sensitive detector. XRR experiments were performed in ambient air. The monochromatic X-ray beam impinged the samples at known grazing angles θ_i from 0.02° to 2.5°, corresponding to 0.005 $Å^{-1}$ to 0.59 $Å^{-1}$ of the component of the momentum transfer vector perpendicular to the surface $q_z = (4\pi/\lambda)\sin(\theta)$. Figure S7 shows reflectivities vs q_z with corresponding fits for $C_{60}C_{18}$-PA and mixed SAMs with 50 % or 30 % $C_{60}C_{18}$-PA on ALD grown AlO_x.

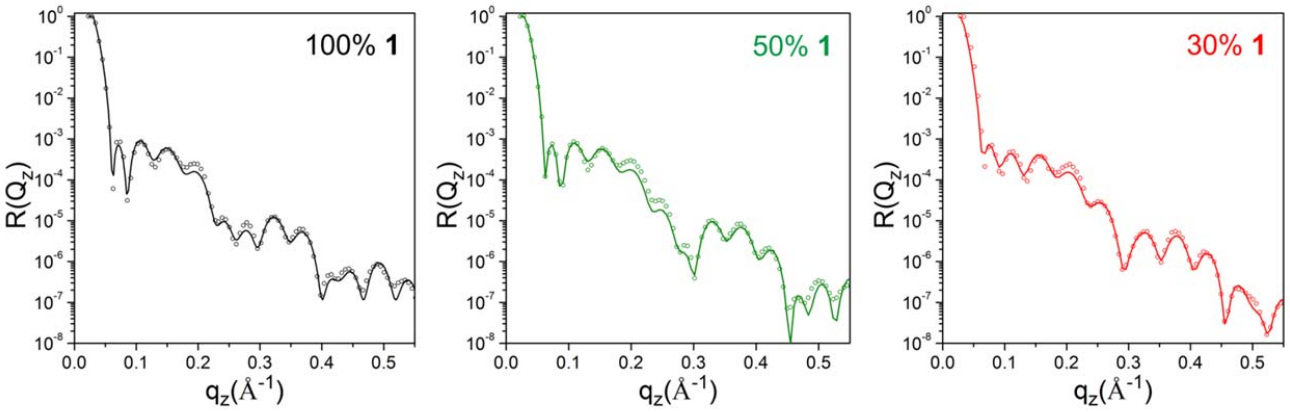

Supplementary Figure S7. Reflectivity data (open circles) and fit results (solid lines) corresponding to model SLD profiles in Fig. S8 for $C_{60}C_{18}$-PA and mixed SAMs with 50 % or 30 % $C_{60}C_{18}$-PA on ALD grown AlO_x.

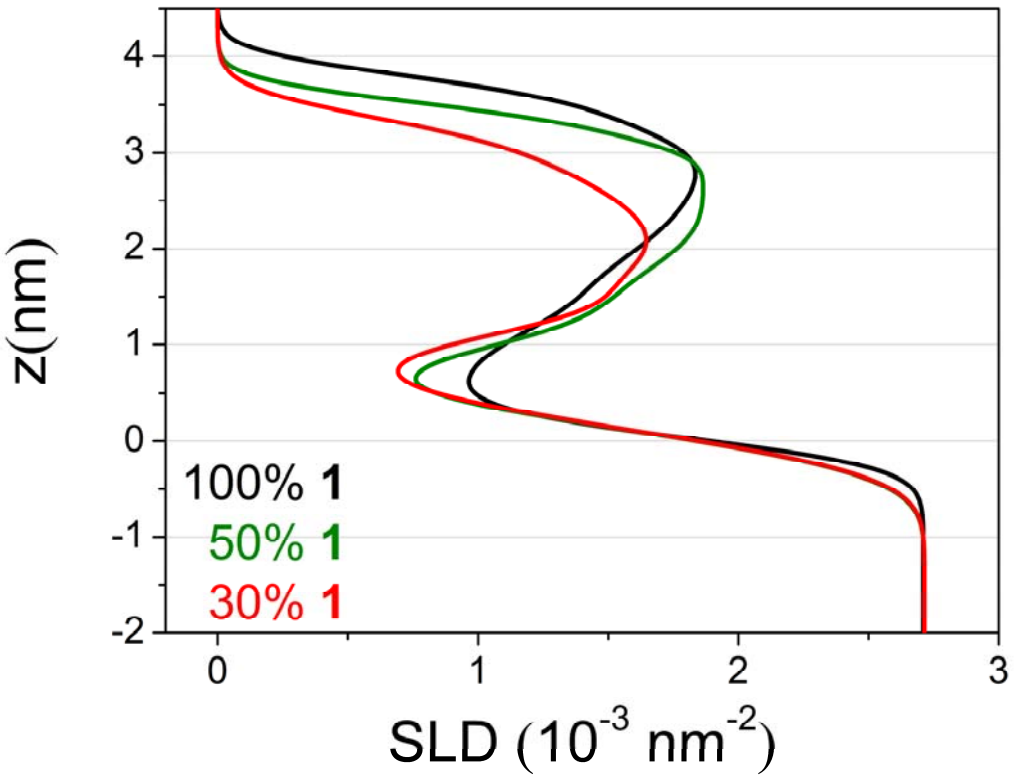

Supplementary Figure S8. Best fit SLD profiles from XRR experiments of pure $C_{60}C_{18}$-PA and mixed SAMs with 50 % or 30 % $C_{60}C_{18}$-PA on ALD grown AlO_x.

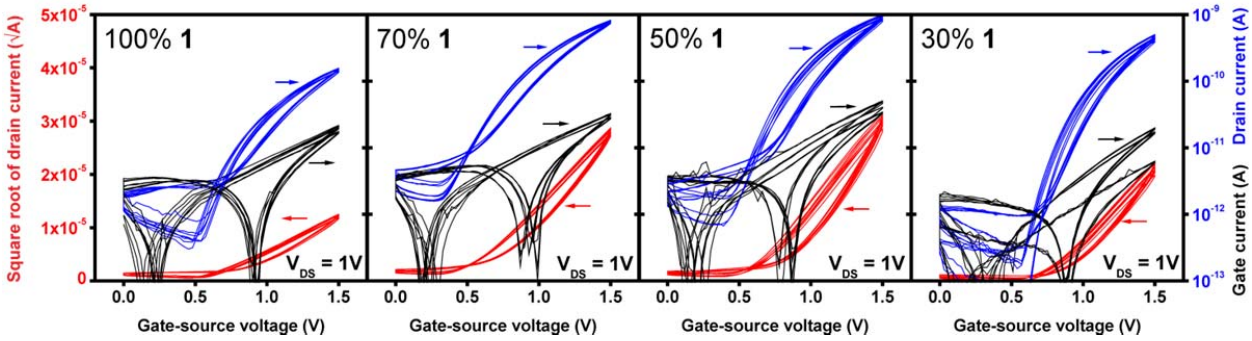

Supplementary Figure S9. Transfer curves of mixed SAMFET devices with different mixing ratios (labelled as % of $C_{60}C_{18}$-PA in the graphs) including square root of the drain current (red), drain current (blue) and gate leakage current (black). Only small differences in leakage currents were measured which are attributed to process related variations of source gate overlaps.

Complete citations for references 3, 14, 16, 20, 21, 22, 23

3. Gelinck, G. H.; Huitema, H. E. A.; van Veenendaal, E.; Cantatore, E.; Schrijnemakers, L.; van der Putten, J. B. P. H.; Geuns, T. C. T.; Beenhakkers, M.; Giesbers, J. B.; Huisman, B.-H.; Meijer, E. J.; Benito, E. M.; Touwslager, F. J.; Marsman, A. W.; van Rens, B. J. E.; de Leeuw, D. M. *Nat. Mater.* **2004,** *3*, 106-110.

14. Smits, E. C. P.; Mathijssen, S. G. J.; van Hal, P. A.; Setayesh, S.; Geuns, T. C. T.; Mutsaers, K. A. H. A.; Cantatore, E.; Wondergem, H. J.; Werzer, O.; Resel, R.; Kemerink, M.; Kirchmeyer, S.; Muzafarov, A. M.; Ponomarenko, S. A.; de Boer, B.; Blom, P. W. M.; de Leeuw, D. M. *Nature* **2008,** *455*, 956-959.

16. Sirringhaus, H.; Brown, P. J.; Friend, R. H.; Nielsen, M. M.; Bechgaard, K.; Langeveld-Voss, B. M. W.; Spiering, A. J. H.; Janssen, R. A. J.; Meijer, E. W.; Herwig, P.; de Leeuw, D. M. *Nature* **1999,** *401*, 685-688.

20. Ringk, A.; Xiaoran, L.; Gholamrezaie, F.; Smits, E. C. P.; Neuhold, A.; Moser, A.; van der Marel, C.; Gelinck, G. H.; Resel, R.; de Leeuw, D. M.; Strohriegl, P. *Adv. Funct. Mater.* **2012**, 1616-3028.

21. Mathijssen, S. G. J.; Smits, E. C. P.; van Hal, P. A.; Wondergem, H. J.; Ponomarenko, S. A.; Moser, A.; Resel, R.; Bobbert, P. A.; Kemerink, M.; Janssen, R.; de Leeuw, D. M. *Nat. Nano* **2009,** *4*, 674-680.

22. Novak, M.; Ebel, A.; Meyer-Friedrichsen, T.; Jedaa, A.; Vieweg, B. F.; Yang, G.; Voitchovsky, K.; Stellacci, F.; Spiecker, E.; Hirsch, A,; Halik, M. *Nano Lett.* **2010,** *11*, 156-159.

23. Guo, X.; Myers, M.; Xiao, S.; Lefenfeld, M.; Steiner, R.; Tulevski, G. S.; Tang, J.; Baumert, J.; Leibfarth, F.; Yardley, J. T.; Steigerwald, M. L.; Kim, P. Nuckolls, C. *Proc. Natl Acad. Sci.* **2006,** *103*, 11452-11456.